

The fate of topological-insulator surface states under strong disorder

Gerald Schubert,^{1,2} Holger Fehske,¹ Lars Fritz,³ and Matthias Vojta⁴

¹*Institut für Physik, Ernst-Moritz-Arndt-Universität Greifswald, 17487 Greifswald, Germany*

²*Philips Healthcare, Äyratie 4, 01510 Vantaa, Finland*

³*Institut für Theoretische Physik, Universität zu Köln, 50937 Köln, Germany*

⁴*Institut für Theoretische Physik, Technische Universität Dresden, 01062 Dresden, Germany*

(Dated: January 10, 2018)

Three-dimensional topological insulators feature Dirac-like surface states which are topologically protected against the influence of weak quenched disorder. Here we investigate the effect of surface disorder beyond the weak-disorder limit using large-scale numerical simulations. We find two qualitatively distinct regimes: Moderate disorder destroys the Dirac cone and induces diffusive metallic behavior at the surface. Even more remarkably, for strong surface disorder a Dirac cone reappears, as new weakly disordered “surface” states emerge in the sample *beneath* the disordered surface layer, which can be understood in terms of an interface between a topological and an Anderson insulator. Together, this demonstrates the drastic effect of disorder on topological surface states, which cannot be captured within effective two-dimensional models for the surface states alone.

Topological insulators (TIs) are a novel form of insulators, where topological properties of the band structure lead to the formation of metallic states at the surface [1, 2]. Two-dimensional (2d) TIs were predicted [3, 4] and then realized in quantum-well heterostructures [5]. Subsequently, three-dimensional (3d) generalizations were discussed theoretically [6–8] and realized afterwards, primarily in Bi-based compounds [9, 10]. 3d TIs are characterized by a set of topological quantum numbers, which lead to a classification into strong and weak TIs.

Strong TIs possess low-energy surface states which can be described in terms of massless 2d Dirac electrons, with an odd number of Dirac cones per surface. Remarkably, these surface states are topologically protected against the influence of disorder due to their helical nature: The spin-momentum locking of the Dirac theory implies that the states \vec{k} and $-\vec{k}$ have opposite spin. This in turn suppresses the lowest-order matrix element for backscattering, $\vec{k} \rightarrow -\vec{k}$, leading to the absence of weak localization for weak potential disorder. What about strong disorder? Theoretical results obtained within 2d continuum Dirac models suggest that such states remain metallic even for arbitrarily large disorder: The beta-function describing the renormalization-group flow of the conductivity is always positive [11–13]. However, by construction the applicability of these effective theories to TI surface states is restricted to energies much smaller than the bulk gap, Δ , and the effect of surface disorder with a strength $\gamma \gtrsim \Delta$ can therefore not be captured. Intuitively, this is because strong impurities will influence both surface and bulk states, causing a non-trivial coupling between the two which cannot be described by a theory for surface states alone.

To the best of our knowledge, the effect of strong surface disorder has only been discussed locally for isolated impurities [14], but the global fate of TI surface states under moderate or strong disorder is not known. This issue is not only of fundamental interest in order to un-

derstand the range and limitations of “topological protection”, but is also of enormous practical relevance: Impurity potentials can easily be in the energy range of 1 eV, thereby exceeding typical band gaps of 3d TIs, e.g. 0.3 eV for Bi_2Se_3 . Moreover, surfaces are often intrinsically disordered, and in addition can be easily disordered intentionally to perform controlled studies of disorder effects. Therefore, non-perturbative theoretical studies of surface disorder are clearly called for.

In this paper, we present a comprehensive study of the effect of surface disorder on 3d TIs by means of large-scale numerical simulations of a 3d lattice model. Our central results can be summarized as follows: Topological protection is only operative for disorder strengths which are small compared to the bulk gap, $\gamma \ll \Delta$. For moderate disorder, $\gamma \sim \Delta$, the surface layer instead shows diffusive metallic behavior, and the momentum-space Dirac-like structure of its states is lost. Moreover, low-energy states start to significantly penetrate into the sample. For strong disorder, $\gamma \gg \Delta$, states in the surface layer become strongly localized, but new weakly disordered metallic states appear which reside primarily in the first inward layer of the sample. Remarkably, these states display a clear Dirac dispersion, suggesting that they can be interpreted as metallic states at the interface between a TI and a strong Anderson insulator (AI).

Our calculations demonstrate that already moderate disorder on TI surfaces requires to consider physics beyond effective 2d Dirac models. On the application side, we propose that strong disorder can be used for nanstructuring of TI devices: Disordered layers in a TI crystal act as atomic-scale barriers which cut the TI.

Model and Methods. As a minimal model for a 3d TI we take four bands in a cubic lattice of N sites, which may also be considered as an effective model for strained 3d HgTe and for insulators of the Bi_2Se_3 family [6, 15, 16]. The Hamiltonian can conveniently be expressed in terms of the identity, Γ^0 and four Dirac matrices Γ^a , $\Gamma^{(1,2,3,4)} =$

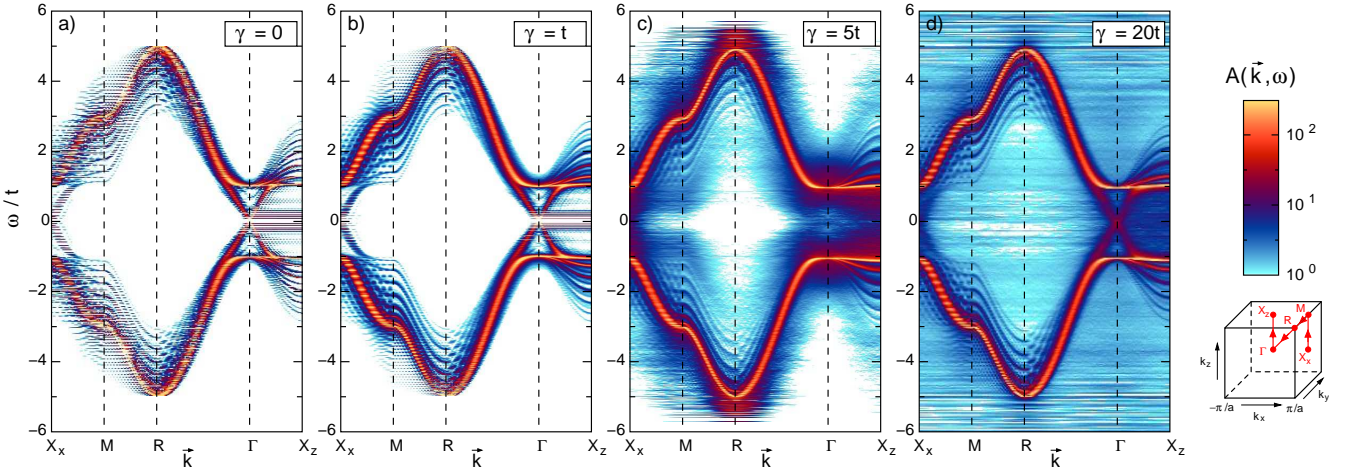


Figure 1: (Color online) Spectral function $A(\vec{k}, \omega)$, Eq. (2), along a path in the 3d Brillouin zone, obtained by ED for the TI model (1) on a $16 \times 16 \times 33$ lattice with open boundaries. Histogram binning has been employed on the ω axis, with bin width $t/50$. The strength of the surface disorder γ increases from a) to d). In the clean case, $\gamma = 0$, bulk states exist for $|\omega| \geq t$, while surface Dirac cones appear near surface momenta $(0, 0)$, as is nicely visible e.g. near $\vec{k} = \Gamma$ [18]. (The small gap at Γ is a finite-size effect, while the ‘‘shadow’’ bands originate from the open boundary conditions.) The surface Dirac cones are destroyed for moderate disorder, $\gamma = 5t$, but re-appear for large disorder, $\gamma = 20t$.

$(\mathbb{1} \otimes s_z, -\sigma_y \otimes s_x, \sigma_x \otimes s_x, -\mathbb{1} \otimes s_y)$ where s (σ) Pauli matrices refer to orbital (spin) space:

$$\mathcal{H} = -t \sum_{n,j=1,2,3} \left(\Psi_{n+\hat{e}_j}^\dagger \frac{\Gamma^1 - i\Gamma^{j+1}}{2} \Psi_n + \text{H.c.} \right) + \sum_n \Psi_n^\dagger (\epsilon_n \Gamma^0 + m \Gamma^1) \Psi_n. \quad (1)$$

Ψ_n is a four-component spinor at site n , t is the hopping amplitude and m a parameter which tunes the band structure. The model describes a weak TI with two Dirac cones per surface for $|m| < t$, a strong TI with a single Dirac cone per surface for $t < |m| < 3t$, and a conventional band insulator for $|m| > 3t$. Our numerical results below are obtained for $m = 2t$, where the bulk band gap is $\Delta = 2t$.

We implement quenched disorder via random on-site energies ϵ_n drawn from a uniform box distribution with width γ . For most of the paper, we will be concerned with surface disorder, i.e., $\epsilon_n \in [-\gamma/2, \gamma/2]$ for sites n on each surface of the sample, and $\epsilon_n = 0$ otherwise.

Using state-of-the-art exact diagonalization (ED) routines [17] we calculate $\{|m\rangle\}$, the two-fold Kramers degenerate eigenstates of \mathcal{H} (1). Those can be visualized in both momentum and position space, via the momentum-resolved spectral function

$$A(\vec{k}, \omega) = \sum_{j=1}^4 \sum_{m=1}^{4N} |\langle m | \psi(\vec{k}, j) \rangle|^2 \delta(\omega - \omega_m) \quad (2)$$

and the local density of states (LDOS)

$$\rho_n(\omega) = \sum_{j=1}^4 \sum_{m=1}^{4N} |\langle m | \psi(\vec{r}_n, j) \rangle|^2 \delta(\omega - \omega_m). \quad (3)$$

Here $\langle \vec{e}_n^{(s)} \otimes \vec{e}_j^{(b)} | \psi(\vec{k}, j') \rangle = \exp(i\vec{k} \cdot \vec{e}_n^{(s)}) \delta_{jj'}$ is a Bloch state and $\langle \vec{e}_n^{(s)} \otimes \vec{e}_j^{(b)} | \psi(\vec{r}_{n'}, j') \rangle = \delta_{nn'} \delta_{jj'}$ a Wannier state, where $|\vec{e}_n^{(s)}\rangle$ and $|\vec{e}_j^{(b)}\rangle$ denote the canonical basis vectors of position and bandindex space, respectively.

Momentum-resolved spectral function. In Fig. 1, we start by presenting results for $A(\vec{k}, \omega)$ along a path following the high-symmetry directions of the *bulk* Brillouin zone. In the clean case, Fig. 1a, bulk states exist at energies $|\omega| \geq t$, and sub-gap surface states are clearly visible: For the model (1) with $m = 2t$ the Dirac cone is located at the surface momentum $\Gamma_s = (0, 0)$ and consequently shows up in $A(\vec{k}, \omega)$ at 3d momenta \vec{k} which equal Γ_s after projection onto the respective surface, e.g., at Γ [18].

While for weak surface disorder, Fig. 1b, the spectral function has changed rather little (apart from minor broadening effects), the picture is drastically altered for moderate disorder in Fig. 1c, where for $\gamma = 5t$ the typical ϵ_n is somewhat larger than the bulk gap. As expected, the bulk states are well defined, but any sub-gap states have lost their momentum-space structure. As will become clear below, the surface states have acquired diffusive character. Finally, Fig. 1d is astonishing, as it shows that sub-gap states with a well-defined Dirac dispersion re-appear for strong surface disorder, $\gamma = 20t$.

Local density of states. More information can be extracted from the LDOS $\rho_n(\omega)$ [21]. Fig. 2 displays the LDOS for the two outer layers (surface and first inward layer) of a finite system at $\omega = 0$, i.e., in the middle of the bulk gap [22]. $\rho_n(\omega)$ can further be used to construct the LDOS probability distribution $f[\rho_n(\omega)]$ [23], i.e., a histogram of LDOS values at a fixed energy ω , for specific parts of the sample. Fig. 3 shows such layer-resolved

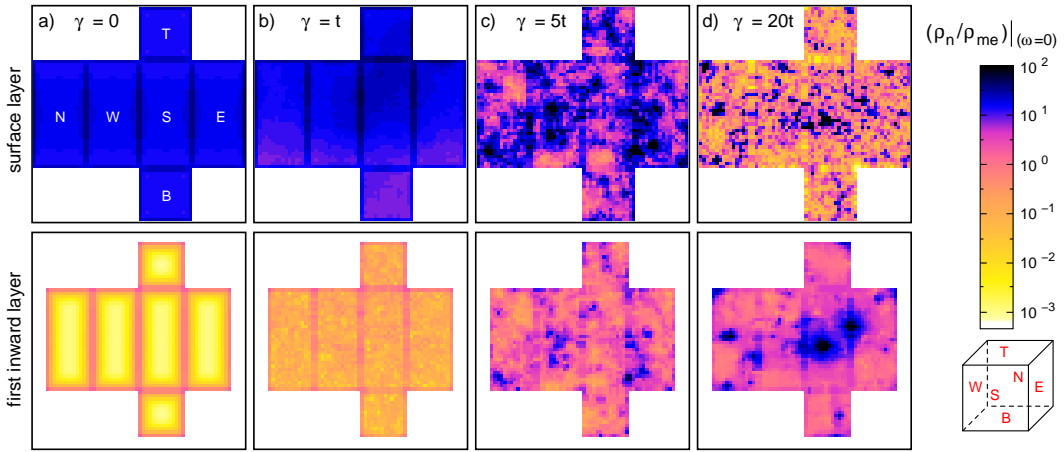


Figure 2: (Color online) Spatially resolved LDOS (3) in the middle of the bulk gap, $\rho_n(\omega=0)$, shown for the surface (top row) and the first inward layer (bottom row) of a $16 \times 16 \times 33$ lattice [21]. ρ is normalized to the mean DOS of an extended *bulk* state, $\rho_{\text{me}} = 1/(4N)$, such that the weight of surface states scales as $N^{1/3}$. Each panel shows the 6 faces according to the scheme in the lower right corner; the strength of the surface disorder γ increases from left to right. While in the clean case, $\gamma = 0$, surface states penetrate the bulk only slightly, this changes already for moderate disorder, $\gamma = 5t$. For $\gamma = 20t$ tendencies of localization on the outer shell are visible, whereas weakly disordered states appear in the first inward shell.

histograms for $\rho_n(\omega=0)$.

In the clean case, Figs. 2a and 3a, we have homogeneous surface states, with the weight being located almost exclusively in the outermost layer. These states are

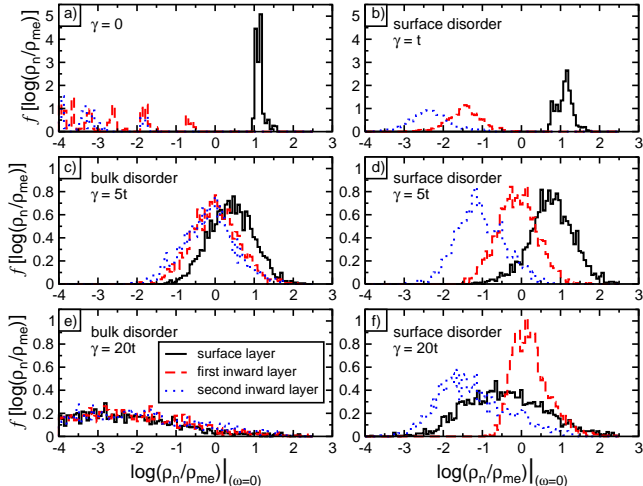


Figure 3: (Color online) Distribution of the in-gap LDOS, $\rho_n(\omega=0)/\rho_{\text{me}}$, for the surface and two next inward layers. Panels b,d,f show different strengths γ of surface disorder, and panels c,e show bulk disorder, i.e., all $\epsilon_n \in [-\gamma/2, \gamma/2]$ for comparison. While the clean case a) has sizeable low-energy LDOS only on the outer layer, weight is distributed to the inner layers with increasing disorder. For strong surface disorder, panel f), the broad distribution for the outer layer indicates localization, while disorder effects are much weaker on the high-intensity first inward layer. In contrast, for bulk disorder the broad LDOS distribution essentially coincides for all layers (surface states are destroyed) and indicates diffusive metallic behavior in c) and localization in f).

only weakly perturbed for $\gamma = t$, Figs. 2b and 3b, consistent with topological protection (although the weight on the first inward layer is seen to increase).

Moderate surface disorder, $\gamma = 5t$, significantly redistributes part of the weight of the in-gap states from the surface to the first inward layer (and even to the second inward layer), Figs. 2c and 3d. Moreover, the states become inhomogeneous, and the LDOS distribution significantly broadens. These are clear signatures of diffusive metallic behavior – this appears consistent with the fact that a 3d TI under influence of moderate *bulk* disorder becomes a diffusive metal [19, 20]. (The latter is nicely visible in Fig. 3c, which shows disordered low-energy states in all layers for a bulk $\gamma = 5t$.) We conclude that, for surface disorder, low-energy surface states do exist for $\gamma = 5t$, but their momentum-space Dirac structure is lost, consistent with Fig. 1c.

We now turn to strong surface disorder, $\gamma = 20t$. Here, the main weight of the low-energy states has been pushed into the sample (!) to the first inward layer, Fig. 3f. In contrast, the LDOS in the surface layer is small with a very broad distribution, corresponding to the “fragmented” real-space structure in Fig. 2d. The surface layer thus shows a clear tendency towards strong Anderson localization. (This conclusion is again supported by the corresponding result for bulk disorder, Fig. 3e, signalling bulk AI behavior [24].) At the same time, the first inward layer displays a much narrower LDOS distribution, i.e., is only weakly affected by disorder (recall that the ϵ_n are zero here). Together with the data in Fig. 1d, this shows that metallic low-energy states have emerged in the first inward layer and exhibit a well-defined Dirac structure in momentum space, much like

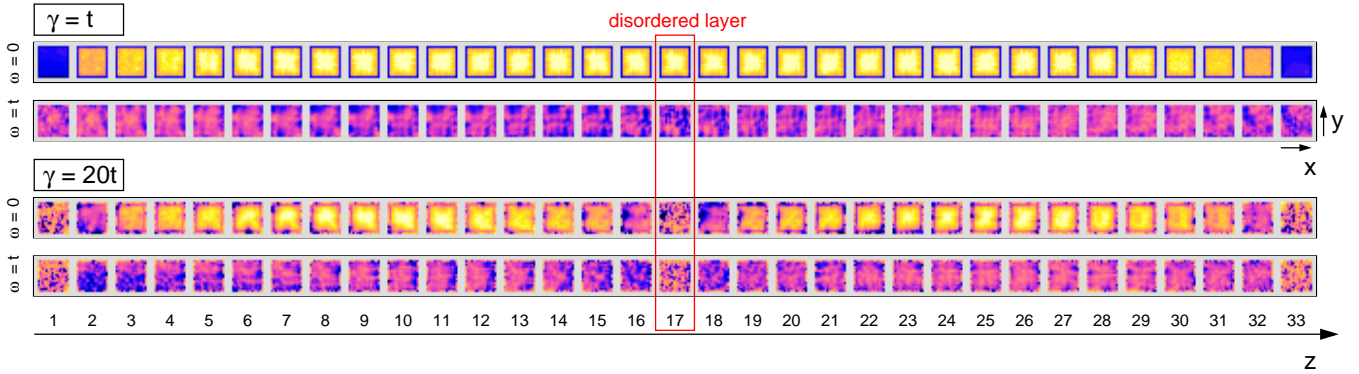


Figure 4: (Color online) Spatially resolved LDOS at energies $\omega = 0$ and t for a $16 \times 16 \times 33$ sample with both surface and midplane disorder, for disorder strengths $\gamma = t$ (top) and $\gamma = 20t$ (bottom). The individual panels show the LDOS slice-by-slice for the entire sample. While weak disorder leaves the physics of the clean sample untouched, strong disorder leads to localization on the surfaces and in the midplane, and new weakly disordered sub-gap states appear both in layers 2 and 32 and in layers 16 and 18 adjacent to the midplane: The disordered midplane has cut the TI into two.

the surface states of the clean sample. The situation thus can be interpreted as an interface between a TI and an AI (which here consists of the surface layer only), with TI interface states forming in the outermost layer of the clean TI.

In the limit of large γ , the behavior can be rationalized by noting that the surface sites with $|\epsilon_n| \gg t$ effectively decouple from the bulk, their only effect being to introduce an effective disorder in the first inward layer of strength t^2/γ , i.e., a smaller TI with weak surface disorder obtains.

Relation to surface Dirac theories. Given the drastic effects of disorder on TI surface states, a comment on disorder effects in 2d Dirac theories is in order. Recent work [11–13] has shown that even strong disorder *cannot* localize electrons of a single Dirac cone, which has lead to the notion of a supermetal and self-organized criticality in the presence of interactions. However, these theories are constructed in the continuum such that the cutoff energy of the Dirac spectrum is the largest energy scale. Therefore lattice effects are not captured, and it is precisely lattice effects which are responsible for strong localization in the limit of strong on-site disorder. (For TIs, such lattice effects include the coupling to sites away from the surface layer.)

We conclude that the applicability of 2d Dirac theories to TI surface states is limited to energy scales small compared to the bulk gap Δ , and thus our results are not in contradiction to those of Refs. 11, 12. Parenthetically, we note that attempts to study 2d *lattice* models with a single Dirac cone are usually hampered by the fermion doubling problem which can only be circumvented in special cases with broken time-reversal symmetry [25]. Therefore, treating the full 3d model as done here is indispensable.

Midplane disorder: How to cut a TI. We can use the insights gained above for an “experiment”: If a single

strongly disordered layer, simulating an AI, produces new Dirac interface states in the TI, this can be used to effectively *cut* a TI. To this end, we introduce on-site disorder selectively in one central layer (or midplane) of the TI, Fig. 4. If this disorder is strong, $\gamma = 20t$, the midplane shows signatures of Anderson localization, and new low-energy states appear to the left and right of the midplane. From Fig. 4 one can deduce that these layers show the same characteristics as the layers adjacent to the disordered surfaces.

Our simulated sample thus represents a layered structure AI–TI–AI–TI–AI (the two outer AI on the sample surface), with interface states bounding both pieces of TI. (We have checked that the properties remain robust if the number of disordered layers is increased.) This suggests efficient nanostructuring via disorder: A large TI crystal can be “cut” into multiple TIs, preserving the single-crystalline structure, by intentionally disordering a few atomic layers, e.g., via irradiation, which then form barriers with new interface states.

Conclusions. By large-scale numerics we have demonstrated that surface disorder can strongly disturb surface states of 3d TIs, such that their description in terms of a 2d Dirac theory breaks down: Topological protection is only relevant for weak disorder, while disorder with a strength comparable to or larger than the bulk gap first leads to diffusive metallic behavior and then to Anderson localization at the surface. In the latter case, the emerging interface between a TI and an AI comes with new low-energy interface states, with properties similar to the surface states of a clean TI interfacing vacuum – the physics of these interface states clearly deserves further studies.

STM experiments have already detected strong perturbations of surface states by isolated impurities [26], and experiments on more disordered surfaces can be used to confirm our predictions.

We thank A. Altland, F. Evers, and C. Timm for discussions. This research was supported by the DFG through SPP1459, SFB608, FOR960, and FR2627/3-1.

[1] M. Z. Hasan and C. L. Kane, *Rev. Mod. Phys.* **82**, 3045 (2010).

[2] X.-L. Qi and S.-C. Zhang, *Rev. Mod. Phys.* **83**, 1057 (2011).

[3] C. L. Kane and E. J. Mele, *Phys. Rev. Lett.* **95**, 226801 (2005).

[4] B. A. Bernevig, T. L. Hughes, S. C. Zhang, *Science* **314**, 1757 (2006).

[5] M. König *et al.*, *Science* **318**, 766 (2007).

[6] L. Fu, C. L. Kane, and E. J. Mele, *Phys. Rev. Lett.* **98**, 106803 (2007).

[7] J. E. Moore and L. Balents, *Phys. Rev. B* **75**, 121306 (2007).

[8] R. Roy, *Phys. Rev. B* **79**, 195322 (2009).

[9] D. Hsieh *et al.*, *Nature* **460**, 1101 (2009).

[10] C. Brüne *et al.*, *Phys. Rev. Lett.* **106**, 126803 (2011).

[11] J. H. Bardarson, J. Tworzydlo, P. W. Brouwer, and C. W. J. Beenakker, *Phys. Rev. Lett.* **99**, 106801 (2007).

[12] K. Nomura, M. Koshino, and S. Ryu, *Phys. Rev. Lett.* **99**, 146806 (2007).

[13] P. M. Ostrovsky, I. V. Gornyi, and A. D. Mirlin, *Phys. Rev. Lett.* **105**, 036803 (2010).

[14] A. M. Black-Schaffer and A. V. Balatsky, preprint arXiv:1110.5149; preprint arXiv:1202.4872.

[15] X. Dai, T. L. Hughes, X.-L. Qi, Z. Fang, and S.-C. Zhang, *Phys. Rev. B* **77**, 125319 (2008).

[16] M. Sitte, A. Rosch, E. Altman, and L. Fritz, preprint arXiv:1110.1363.

[17] A. Weiße and H. Fehske, *Lect. Notes in Physics* **739**, 529 (2008); DOI: 10.1007/978-3-540-74686-7-18

[18] Surface states have reduced weight in $A(\vec{k}, \omega)$ as compared to bulk states, as they only occupy L^2 sites in a sample of size L^3 .

[19] S. Ryu and K. Nomura, preprint arXiv:1109.2942.

[20] H.-M. Guo, G. Rosenberg, G. Refael, and M. Franz, *Phys. Rev. Lett.* **105**, 216601 (2010).

[21] Results are derived from a single realization of disorder to emphasize the typical behavior of an individual sample.

[22] The plots of $\rho_n(\omega)$ show the cumulated weight at site n of the two degenerate eigenstates of \mathcal{H} at the energy closest to a given ω .

[23] G. Schubert, J. Schleede, K. Byczuk, H. Fehske, and D. Vollhardt, *Phys. Rev. B* **81**, 155106 (2010).

[24] Our samples are too small for an accurate detection of Anderson localization.

[25] F. D. M. Haldane, *Phys. Rev. Lett.* **61**, 2015 (1988).

[26] Z. Alpichshev *et al.*, preprint arXiv:1108.0022.